Bipedal Robotic Running with Partial Hybrid Zero Dynamics and Human-Inspired Optimization

Huihua Zhao, Shishir Nadubettu Yadukumar and Aaron D. Ames

Abstract— **This paper presents a method for achieving stable "human-like" running in simulation by using human-inspired control. Data from human running experiments are processed, analyzed and split into the two domains: stance phase and flight phase. By examining this data, we present a set of outputs, i.e., functions of the kinematics, which appear to represent human running; moreover, we show that this output data can be described by the time-solution to a linear spring-mass-damper—termed the *canonical locomotion function*. This observation motivates the construction of a human-inspired optimization that determines the parameters of the canonical locomotion function that provide the best fit of the human data while simultaneously enforcing *partial hybrid zero dynamics*, i.e., that the human outputs track the canonical locomotion functions even through impacts. The main result is a method for numerically solving this optimization problem that provably results in stable robotic running. Simulation results are presented that demonstrate the "human-like" robotic running obtained through this procedure.**

I. INTRODUCTION

Running is defined as a forward motion with switching between single support and flight phases [8]. Considering high speed locomotion, running displays more mobility and energy efficiency compared to walking. In the field of humanoid bipedal locomotion study, the human body has always been the most widely used reference model. With 57 muscles utilized in human locomotion [22], this system is far too complex to replicate with any hardware and computational capabilities. However, despite the obvious challenge it presents, a substantial amount of work has been devoted to achieving human-like bipedal locomotion. In particular, following the work on hopping robots [21], numerous studies have been devoted on the analysis of bipedal running. Passive running was studied in [17]; running with ZMP can be found in [28]; and optimal trajectory tracking was analyzed in [16]. There are also numerous physical robots which have experimentally achieved running. The hopping robots in [19] can perform various locomotion behaviors including running. Honda ASIMO can run with ZMP control technology [1]. A relatively recent hopping robot ATRIAS 2, which is a physical realization of spring mass model (SLIP model), can hop with a flight phase under the support of a boom [14]. The underactuated bipedal robot MABEL [15] can achieve speed up to 6.8mph of bipedal running.

The main idea underlying this paper (extending recent work by the authors [4], [20] that has proved successful experimentally [3], [27]) is that by looking to human data, certain outputs can be utilized to characterize natural human running. By tracking these outputs, as represented by specific running functions, a bipedal robot can achieve remarkably "human-like" running. With this motivation in mind, we first discuss the analysis of the human running data by showing that certain outputs of human running data can be characterized by the time-solution of a linear spring-mass-damper system under constant force; this *canonical locomotion function*, which has been proved to work well for other motion primitives in [20], provides accurate fits to the outputs for both the stance phase and flight phase of human running data with high correlations.

To construct controllers based upon these observations, a multi-domain hybrid system model is constructed to model a bipedal robot and, specifically, the two phases presented in running. Then, we introduce a *human-inspired* controller with feedback linearization that drives the outputs of the robot, on both phases, to the outputs of the human as represented by the canonical locomotion function. The notion of the *partial zero dynamics* surface is then introduced to achieve a low dimension representative of the hybrid nonlinear system, i.e., the system is explicitly predictable without using integration if the system is on the surface [25]. The main results of this paper are the conditions that ensure partial *hybrid* zero dynamics, i.e., that the partial zero dynamics surface is invariant through impact, which yields a more robust system. This allows us to present a human-inspired optimization problem that enforces these conditions to achieve a stable running gait [4], [20] while simultaneously finding the good fits of the human data. These formal results are verified through simulation by numerically solving this optimization problem, with the end result being stable "human-like" bipedal robotic running.

The structure of this paper is as following. In Sect. II, the processing of human running data will be discussed. The domain breakdown will be stated and the outputs of human running are selected. Then, we model the running bipedal system as a multi-domain hybrid system and derive the dynamics for the system in Sect. III. Development of controllers are discussed explicitly in Sect. IV for both phases of running. We term this controller the human-inspired controller due to the fact that it is derived from human data directly. To obtain the parameters of the controller, human-inspired optimization with constraints that guarantee partial hybrid zero dynamics is discussed in detail in Sect. V. Finally, the simulation result and conclusion remarks will be stated in Sect. VI.

II. HUMAN RUNNING DATA

This section will be devoted to discussing human running data in detail. It will start with a description of the experimental human data, and then characterize running in terms of the *canonical locomotion function* [4].

Running Data. The human running data was obtained through a high speed motion capture system, the set up details of which can be found in [3]. A particular domain break method in [12] has been applied to specify a single step which contains a stance phase and a flight phase. Fig. 1 shows the domain break down of one step for one of the subjects. In order to reduce the noise accrued by the sensors and to reduce the complexity of the signals, we average the outputs of all six subjects to obtain a new set of data called the mean human data (details can be found in [12] and the measurements for subjects and the mean model are taken from [20]).
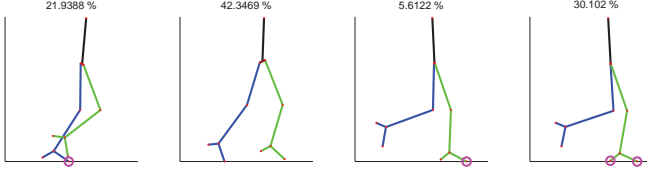

Fig. 1: Domain breakdown of one step evolving from left to right of one subject along with the time spent in each domain is shown here. The red circles indicate ground contact.

Human Outputs. We seek human running outputs which are functions of the joint angles, while satisfying specified criteria, e.g., they should be mutually exclusive [12]. A total of four outputs are required for a fully actuated 4-DOF robot model. Note that in the flight phase, we have 6-DOF since the stance foot is not fixed to the ground. Analysis of the human data yields the following four outputs which seem to describe the human locomotion system (see Fig.3(c)):

1. the linearized forward position of the hip,

$$\delta p_{hip} = -\theta_{sf}L_c + (-\theta_{sf} - \theta_{sk})L_t,$$

where L_c and L_t are the lengths of the calf and thigh, respectively. θ_{sf} is the stance foot angle;

2. the non-stance hip angle, θ_{hip}, which is the angle measured from non-stance thigh to stance thigh;
3. the stance knee angle, θ_{sk};
4. the non-stance knee angle, θ_{nsk}.

Importantly, these outputs have been successfully used to achieve physical robotic walking [3], [27].

Canonical Locomotion Function. It was shown in [4], [12] that certain human outputs can be characterized by the response of a linear spring-mass-damper system for walking and stair climbing, which has been named as *canonical walking function*. Analysis of the data shows that the specific outputs of running data can also be represented with the same function which we termed *canonical locomotion function*:

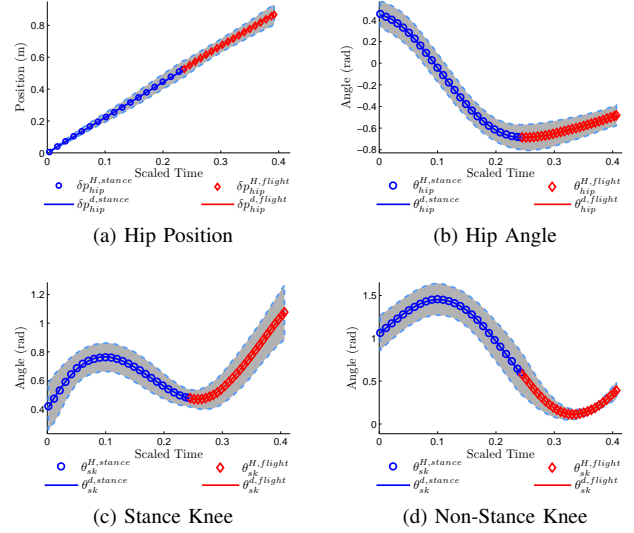$$y_H(t) = e^{-\alpha_1 t}(\alpha_2 \cos(\alpha_3 t) + \alpha_4 \sin(\alpha_3 t)) + \alpha_5, \quad (1)$$

(a) Hip Position (b) Hip Angle

(c) Stance Knee (d) Non-Stance Knee

Fig. 2: Fitted canonical human functions (solid) and the corresponding mean human data of running (dashed).

where the parameters α_1-α_5 are parameters of the linear spring-mass-damper equations. For example, the desired non-stance hip angle can be described by the canonical function as $\theta_{hip}^d(t, \alpha_{hip}^i) = y_H(t, \alpha_{hip}^i)$, where $i \in \{s, f\}$ with s standing for stance phase and f standing for flight phase; and $\alpha_{hip}^{\mathbf{s}} = (\alpha_{hip,1}^{\mathbf{s}}, \alpha_{hip,2}^{\mathbf{s}}, \alpha_{hip,3}^{\mathbf{s}}, \alpha_{hip,4}^{\mathbf{s}}, \alpha_{hip,5}^{\mathbf{s}})$. We then group the parameters of other outputs in each domain to yield $\alpha^i = (\alpha_{hip}^i, \alpha_{sk}^i, \alpha_{nsk}^i)$. Note that, the forward hip velocity is approximately constant during the whole step (see Fig. 2(a)), thus, motivating us to fit it with a linear function of time $\delta p_{hip}^d(t, v_{hip}) = v_{hip}t$. Combining the parameters for each domain with the velocity of hip, v_{hip}, results in a single vector of parameters: $\alpha = (v_{hip}, \alpha^{\mathbf{s}}, \alpha^{\mathbf{f}}) \in \mathbb{R}^{31}$.

Therefore, to get the α which provides the canonical locomotion function that best fits the mean human data, we propose an optimization problem:

$$\alpha^* = \operatorname*{argmin}_{\alpha \in \mathbb{R}^{31}} \operatorname{Cost}_{\mathrm{HD}}(\alpha), \quad (2)$$

$$\text{s.t} \quad y_j^{d,\mathbf{s}}(t_{j,end}^{H,\mathbf{s}}, \alpha_j^{\mathbf{s}}) = y_j^{d,\mathbf{f}}(t_{j,start}^{H,\mathbf{f}}, \alpha_j^{\mathbf{f}}).$$

where $\operatorname{Cost}_{\mathrm{HD}}(\alpha)$ is the sum of least square errors between canonical functions and human data computed at discrete times with specified weighting [12]. Note that, $j \in \mathrm{Outputs}$; $t_{start}^{\mathbf{s}}$ and $t_{end}^{\mathbf{f}}$ represent the time at the end of stance phase and the start of flight phase, respectively. Therefore, the fitting constraints simply ensure that the desired fitting functions should be continuous between the stance phase and flight phase w.r.t corresponding outputs.

The result of fitting parameters by solving the optimization problem can be seen in Table. I and Fig. 2, from which we can see that the canonical locomotion function can be fitted to the outputs of both phases very well (all correlations are higher than 0.99). Note that, the reason we term the function "canonical locomotion function" is that this function can fit all the outputs of different motion primitives (walking, stair climbing [20] and running) for all the subjects with

high correlation, i.e., it seems to characterize the human locomotion behavior universally. Therefore, this result allows us to make the conclusion in [4], [12] even stronger; namely, that human appears to act like linear spring-mass-damper systems for the outputs considered (see [7], [9], [10], [13]).

III. MODELING OF THE RUNNING BIPED ROBOT

Bipedal running contains both discrete and continuous behavior, and is thus naturally modeled as *hybrid systems* (see [3], [24]). In this section, the multi-domain hybrid system for modeling a bipedal running robot is introduced with the alternative phases "stance" when the robot is in contact with the ground and "flight" when the robot is in the air. We refer the reader to [5] for the specifics of modeling multi-domain hybrid systems on graphs. We also note that we implicitly assume the standard assumptions on the robot such as no slipping (see [25] for more details).

Hybrid System Model. The hybrid control system modeling a running robot (with point feet) is given by

$$\mathscr{HC} = (\Gamma, \mathcal{D}, \mathcal{U}, S, \Delta, FG). \tag{3}$$

where

- $\Gamma = (V, E)$ is a *directed cycle*, with $V = \{\mathbf{s}, \mathbf{f}\}$, where $\mathbf{s}$ and $\mathbf{f}$ stand for stance phase and flight phase, respectively, and $E = \{e_1 = \{\mathbf{s} \to \mathbf{f}\}, e_2 = \{\mathbf{f} \to \mathbf{s}\}\}$,
- $\mathcal{D} = \{D_\mathbf{s}, D_\mathbf{f}\}$ is a set of *domains of admissibility*,
- $\mathcal{U} = \{\mathcal{U}_\mathbf{s}, \mathcal{U}_\mathbf{f}\}$ is the set of *admissible controls*,
- $S = \{\mathcal{S}_{\mathbf{s} \to \mathbf{f}}, \mathcal{S}_{\mathbf{f} \to \mathbf{s}}\}$ is a set of *guards*,
- $\Delta = \{\Delta_{\mathbf{s} \to \mathbf{f}}, \Delta_{\mathbf{f} \to \mathbf{s}}\}$ is a set of *reset maps*,
- $FG = \{(f_\mathbf{s}, g_\mathbf{s}), (f_\mathbf{f}, g_\mathbf{f})\}$ with (f_i, g_i) a *control system* on D_i, i.e., $\dot{x} = f_i(x) + g_i(x)u$ for $x \in \mathcal{D}_i$ and $u \in \mathcal{U}_i$.

The specific details on how the individual elements of this model are constructed will be presented in this section.

Continuous Dynamics: The configurations of both phases are depicted in Fig. 3. In particular, the generalized coordinates $q = (q_b, p_x, p_z)$ comprises the vector of body coordinates $q_b = (\theta_1, \theta_2, \theta_3, \theta_4)^T$ and p_x, p_z, which are the forward and vertical Cartesian coordinates of the stance foot, denoting the biped's absolute position. Therefore, with the Euler-Lagrange method, the equations of motion (EOM) of both the phases can be stated.

Flight phase: The dynamics of flight phase can be stated as:

$$D(q)\ddot{q} + H(q, \dot{q}) = B_\mathbf{f}(q)u^\mathbf{f} \tag{4}$$
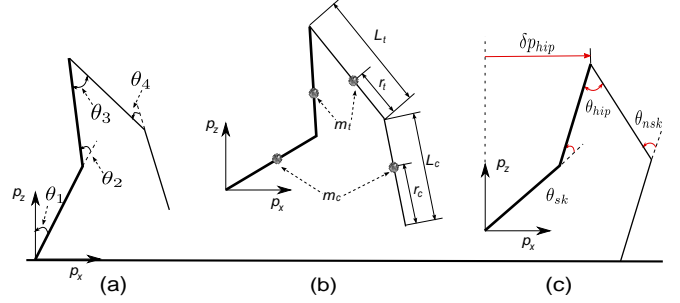

Fig. 3: (a) is the modeling configuration; (b) is the mass and length distribution; (c) shows the virtual constraints.

where we have torque distribution map $B_\mathbf{f}(q) \in \mathbb{R}^{6 \times 3}$ and $u^\mathbf{f} \in \mathcal{U}_\mathbf{f} = \mathbb{R}^3$, since the robot is underactuated for this phase (torque can only be applied to the stance and non-stance knee and the hip). Note that, we use the standard definition (see [25]) for the specified terms in this equation to simplify the exposition. Manipulation of (4) leads to the affine control system $(f_\mathbf{f}, g_\mathbf{f})$ for the flight phase.

Stance phase: We obtain the dynamics for the stance phase by introducing a Lagrange multiplier to the EOM:

$$D(q)\ddot{q} + H(q, \dot{q}) + A^T(q)\lambda = B_\mathbf{s}(q)u^\mathbf{s} \tag{5}$$

with torque distribution map $B_\mathbf{s}(q_e) \in \mathbb{R}^{6 \times 4}$, $u^\mathbf{s} \in \mathcal{U}_\mathbf{s} = \mathbb{R}^4$ considering the fully actuation in this domain. $A^T(q) \in \mathbb{R}^{6 \times 2}$ is the set of two velocity constraints corresponding to the holonomic constraints $\ddot{p}_x = 0$ and $\ddot{p}_z = 0$, and λ is the corresponding Lagrange multiplier (the equation can be found [18]). Manipulation of (5) yields the affine control system $(f_\mathbf{s}, g_\mathbf{s})$ of the stance phase.

Transition Dynamics: The transition dynamics determine the domains and guards, $\mathcal{D}$ and S, for each domain. The flight phase domain consists of the states where the height of the non-stance foot $h_{ns}(q) \geq 0$ and stance foot $h_s(q) \geq 0$.

$$D_\mathbf{f} = \{(q, \dot{q}) \in T\mathcal{Q} : h_i(q) \geq 0, \ i \in \{s, ns\}\} \tag{6}$$

And the guard is given by the states where the foot strikes the ground (with a downward velocity), and therefore:

$$\mathcal{S}_{\mathbf{f} \to \mathbf{s}} = \{(q, \dot{q}) \in T\mathcal{Q} : h_{ns}(q) = 0, \ dh_{ns}(q)\dot{q} < 0\} \tag{7}$$

Impacts happen when the non-stance foot hits the ground, i.e., the guard. To compute the discrete dynamics from the impact model from [11] (also see [25]) which assumes that an impulsive force is applied at the non-stance foot upon impact with the ground that results in a perfectly plastic impact in the system. This allows us to state the reset map:

$$\Delta_{\mathbf{f} \to \mathbf{s}}(q, \dot{q}) = \begin{bmatrix} \Delta_q q \\ \Delta_{\dot{q}}(q)\dot{q} \end{bmatrix} \tag{8}$$

where Δ_q "switches" the stance and non-stance leg after the impact, and $\Delta_{\dot{q}}(q)$ gives of the post-impact velocity.

For the stance phase, the domain consists of states (and control values) where the foot is on the ground (which is enforced in the dynamics through holonomic constraints),

TABLE I: Fitted parameters for mean human data

		$y_1^d = v_{hip}t,$	$y_2^d = y_H(t)$ given in ([4])					
*	*	v_{hip}	α_1	α_2	α_3	α_4	α_5	Corr
Mean	δp_{hip}^{stance}	2.327	*	*	*	*	*	0.9999
*	δp_{hip}^{flight}	2.440	*	*	*	*	*	0.9998
*	θ_{hip}^{stance}	*	1.319	0.627	15.29	0.023	-0.110	1.0000
*	θ_{hip}^{flight}	*	-6.459	0.285	0.002	0.191	-0.827	0.9998
*	θ_{sk}^{stance}	*	7.502	-0.374	-0.000	0.061	0.916	0.9996
*	θ_{sk}^{flight}	*	11.29	-0.593	5.337	-0.590	1.538	1.0000
*	θ_{nsk}^{stance}	*	-1.953	-0.049	16.31	0.354	0.939	1.0000
*	θ_{nsk}^{flight}	*	13.35	0.134	21.65	-0.313	0.507	0.9999

and the lagrange multiplier associated with the stance foot is negative indicating the foot is pushing into the ground:

$$D_{\mathbf{s}} = \{(q, \dot{q}, u^{\mathbf{s}}) \in T\mathcal{Q} \times \mathcal{U}_{\mathbf{s}} : \lambda(q, \dot{q}, u^{\mathbf{s}}) \leq 0\} \quad (9)$$

The guard consists of the states where the Lagrange multiplier changes sign:

$$\mathcal{S}_{\mathbf{s} \to \mathbf{f}} = \{(q, \dot{q}, u^{\mathbf{s}}) \in T\mathcal{Q} \times \mathcal{U}_{\mathbf{s}} : \lambda(q, \dot{q}, u^{\mathbf{s}}) = 0\} \quad (10)$$

Since no impacts occur as the robot enters the flight phase, the reset map of stance to flight is given as $\Delta_{\mathbf{s} \to \mathbf{f}} = I$.

IV. CONTROLLER DESIGN

Inspired by the objective of achieving human-like running, we need to find a controller u that drives the outputs of the robot to match the corresponding outputs of human, i.e., which guarantees that $y^a(q) \to y^d(t)$ as $t \to \infty$, where y^a is the actual outputs of the robot and y^d are the outputs of human as represented by the canonical locomotion function. Considering the nonlinearity of the robot model, the Input/Output Linearization method in [23] is utilized for the controller design.

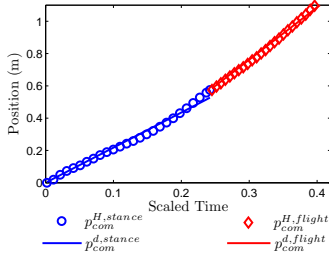**Parameterization of Time** *Autonomous* control has several advantages for the control of bipedal robots, the details

Fig. 4: Human p_{COM} data.

of which can be found in [6]. With this consideration, we introduce a state-based parameterization of time in our system; as is common practice in [25], [26]. Analysis of human data reveals that the forward position of center of mass (COM) evolves in an approximately-linear manner with respect to time in both phases, i.e., $p_{\mathrm{COM}}(t, v_{\mathrm{COM}}) \approx v_{\mathrm{COM}} t$, where p_{COM} denotes the forward position of the COM and v_{COM} denotes the forward velocity of the COM. The forward position of COM of human data along with the fitting can be seen in Fig. 4. Taking advantage of this observation, the following parameterization of time is formed:

$$\tau_i(q) = \frac{p_{\mathrm{COM}}(q) - p_{\mathrm{COM}}(q_i^+)}{v_{\mathrm{COM}}}, \qquad i \in \{\mathbf{s}, \mathbf{f}\} \quad (11)$$

where $p_{\mathrm{COM}}(q_i^+)$ is the forward position of the robot's COM at the beginning of the current step in either the stance or flight phase. Note that we parameterize time in the two domains separately since we control each phase separately.

Control Law Construction. Based on the human canonical locomotion function discussed in Sec. II, we define the full order human-inspired outputs to be:

$$y^i(q) = \begin{bmatrix} y_1(q, \dot{q}) \\ y_2^i(q) \end{bmatrix} = \begin{bmatrix} \delta p_{\mathrm{hip}}(q)\dot{q} - v_{\mathrm{hip}} \\ y_2^a(q) - y_2^d(\tau_i(q), \alpha^i) \end{bmatrix}, i \in \{s, f\} \quad (12)$$

where $y_1(q, \dot{q})$ is the relative degree one output, which is the difference between the actual forward hip velocity $\delta p_{\mathrm{hip}}(q)\dot{q}$ and the desired hip velocity v_{hip}. And $y_2^i(q)$ are the relative

degree two human-inspired outputs which are the difference between the actual relative degree two outputs $y_2^a(q)$ and desired relative degree two outputs $y_2^d(q)$, given as:

$$y_2^a(q) = \begin{bmatrix} \theta_{hip} \\ \theta_{sk} \\ \theta_{nsk} \end{bmatrix}, \quad y_2^d(t, \alpha^i) = \begin{bmatrix} \theta_{hip}^d(t, \alpha_{sk}^i) \\ \theta_{sk}^d(t, \alpha_{sk}^i) \\ \theta_{nsk}^d(t, \alpha_{nsk}^i) \end{bmatrix} \quad (13)$$

With these constructions in mind, we calculate the controllers for the stance and flight phase:

<u>Stance Phase:</u> For the fully actuated stance phase, through Input/Output Linearization, we can define the following control law for the affine control system $(f_{\mathbf{s}}, g_{\mathbf{s}})$ as:

$$u_{(\alpha^{\mathbf{s}}, \varepsilon)}^{\mathbf{s}}(q, \dot{q}) = -\mathcal{A}_{\mathbf{s}}^{-1}(q, \dot{q}) \left(\begin{bmatrix} 0 \\ L_{f_{\mathbf{s}}} L_{f_{\mathbf{s}}} y_2^{\mathbf{s}}(q) \end{bmatrix} \right. \quad (14)$$
$$\left. + \begin{bmatrix} L_{f_{\mathbf{s}}} y_1(q, \dot{q}) \\ 2\varepsilon L_{f_{\mathbf{s}}} y_2^{\mathbf{s}}(q, \dot{q}) \end{bmatrix} + \begin{bmatrix} \varepsilon y_1(q, \dot{q}) \\ \varepsilon^2 y_2^{\mathbf{s}}(q) \end{bmatrix} \right),$$

with control gain ε, L the Lie derivative, and the nonsingular decoupling matrix $\mathcal{A}_{\mathbf{s}}(q, \dot{q})$ (details can be found in [4]).

<u>Flight Phase:</u> For the underactuated flight phase, we only have the relative degree two outputs. Hence, the controller for the affine control system $(f_{\mathbf{f}}, g_{\mathbf{f}})$ is given as:

$$u_{(\alpha^{\mathbf{f}}, \varepsilon)}^{\mathbf{f}}(q, \dot{q}) = \quad (15)$$
$$- \mathcal{A}_{\mathbf{f}}^{-1}(q, \dot{q}) \left(L_{f_{\mathbf{f}}}^2 y_2^{\mathbf{f}}(q_f, \dot{q}_f) + 2\varepsilon L_{f_{\mathbf{f}}} y_2^{\mathbf{f}}(q, \dot{q}) + \varepsilon^2 y_2^{\mathbf{f}}(q) \right),$$

with $\mathcal{A}_{\mathbf{f}}(q, \dot{q}) = L_{g_{\mathbf{f}}} L_{f_{\mathbf{f}}} y_2^{\mathbf{f}}(q, \dot{q})$ the decoupling matrix (in the case of underactuated running). Again, the choice of outputs implies that this matrix is nonsingular.

Hybrid System. From the feedback controllers introduced for both phases, the end result is a hybrid system:

$$\mathscr{H}_{(\alpha, \varepsilon)} = (\Gamma, \mathcal{D}, S, \Delta, F), \quad (16)$$

where Γ, $\mathcal{D}$, S and Δ are as in (3) except now for $D_{\mathbf{s}}$ and $\mathcal{S}_{\mathbf{s} \to \mathbf{f}}$, $u^{\mathbf{s}} = u_{(\alpha^{\mathbf{s}}, \varepsilon)}^{\mathbf{s}}(q, \dot{q})$ making them subsets of $T\mathcal{Q}$ (and not $T\mathcal{Q} \times \mathcal{U}_{\mathbf{s}}$). This implies that, for the Lagrange multiplier in (5), we can write $\lambda(q, \dot{q})$. In addition, $F = \{f_{\mathbf{s}}^{(\alpha^{\mathbf{s}}, \varepsilon)}, f_{\mathbf{f}}^{(\alpha^{\mathbf{f}}, \varepsilon)}\}$ is the set of feedback vector fields where:

$$f_{\mathbf{s}}^{(\alpha^{\mathbf{s}}, \varepsilon)}(q, \dot{q}) = f_{\mathbf{s}}(q, \dot{q}) + g_{\mathbf{s}}(q, \dot{q}) u_{(\alpha^{\mathbf{s}}, \varepsilon)}^{\mathbf{s}}(q, \dot{q}), \quad (17)$$
$$f_{\mathbf{f}}^{(\alpha^{\mathbf{f}}, \varepsilon)}(q, \dot{q}) = f_{\mathbf{f}}(q, \dot{q}) + g_{\mathbf{f}}(q, \dot{q}) u_{(\alpha^{\mathbf{f}}, \varepsilon)}^{\mathbf{f}}(q, \dot{q}), \quad (18)$$

Clearly, each individual vector field depends on ε, and the parameters for their respective domains, $\alpha^{\mathbf{s}}$ and $\alpha^{\mathbf{f}}$. The goal of human inspired optimization is to design the parameters $\alpha = (v_{\mathrm{hip}}, \alpha^{\mathbf{s}}, \alpha^{\mathbf{f}})$ such that the hybrid system $\mathscr{H}_{(\alpha, \varepsilon)}$ has a stable periodic orbit, i.e., a stable running gait, for sufficiently large ε. Since this will be done utilizing the concepts of full and partial zero dynamics, they must first be introduced.

Full and Partial Zero Dynamics. If we begin by considering the fully actuated stance domain, the control law $u^{\mathbf{s}}$ drives the human-inspired outputs $y^i(q, \dot{q}) \to 0$ exponentially with the rate of ε. Therefore, for the *continuous* dynamics, the controller renders the *full zero dynamics surface*:

$$\mathbf{FZ}_{\alpha^{\mathbf{s}}} = \left\{ (q, \dot{q}) \in T\mathcal{Q} : y^{\mathbf{s}}(q, \dot{q}) = \mathbf{0}, L_{f_{\mathbf{s}}^{(\alpha^{\mathbf{s}}, \varepsilon)}} y_2^{\mathbf{s}}(q, \dot{q}) = \mathbf{0} \right\}, \quad (19)$$
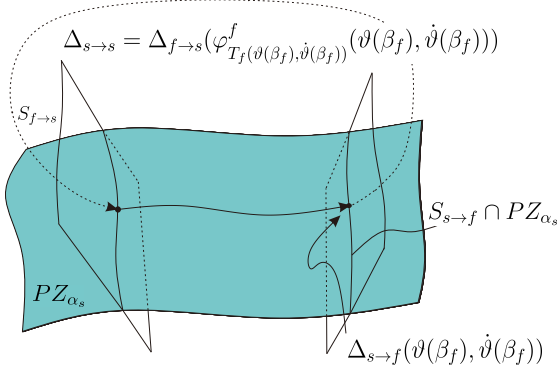
Fig. 5: Geometry of the closed-loop hybrid system of running, where the flight phase and the impact map $\Delta_{\mathbf{f}\to\mathbf{s}}$ are composed to form a generalized impact map $\Delta_{\mathbf{s}\to\mathbf{s}}$.

exponentially stable. However, the invariance of the surface will be disturbed when the system enters the flight phase, and will most possibly not return to the surface after the flight phase (due to impacts in the system and the fact that the flight phase has a different set of controller parameters). Therefore, we want to allow for a "larger" surface as the target for the end of the flight phase dynamics. This motivates the *partial hybrid zero dynamics surface* (PHZD), consisting of the relative degree 2 outputs only and given by:

$$\mathbf{PZ}_{\alpha^i} = \{(q, \dot q) \in T\mathcal{Q} : y_2^i(q) = \mathbf{0}, \; L_{f_i^{(\alpha^i,\varepsilon)}} y_2^i(q, \dot q) = \mathbf{0}\}. \quad (20)$$

Note that, with different DOFs of stance and flight phases, the PHZD surface for each phase will be different. The readers can refer to [25] for more details.

V. Human-Inspired Optimization

In this section, we will discuss the process obtaining a human-inspired controller from the human data via the optimization where the cost function in (2) is used together with *Partial Hybrid Zero Dynamics* constraints. In addition, the parameterization of time and inverse kinematics are introduced such that we can solve the human-inspired optimization.

PHZD Optimization for Running. The goal of this paper is to find the controller parameters α^* by solving the following *human-inspired* constrained optimization problem that achieves partial hybrid zero dynamics on the stance phase:

$$\alpha^* = \underset{\alpha \in \mathbb{R}^{31}}{\mathrm{argmin}} \; \mathrm{Cost}_{\mathrm{HD}}(\alpha) \quad (21)$$

$$\text{s.t} \quad \Delta_{\mathbf{s}\to\mathbf{s}}(\mathcal{S}_{\mathbf{s}\to\mathbf{f}} \cap \mathbf{FZ}_{\alpha^{\mathbf{s}}}) \subset \mathbf{PZ}_{\alpha^{\mathbf{s}}}. \quad \text{(PHZD)}$$

where here

$$\Delta_{\mathbf{s}\to\mathbf{s}}(q, \dot q) = \Delta_{\mathbf{f}\to\mathbf{s}}(\varphi^{\mathbf{f}}_{T_{\mathbf{f}}(q,\dot q)}(q, \dot q)) \quad (22)$$

with $\varphi^{\mathbf{f}}$ the solution to the vector field $f_{\mathbf{f}}^{(\alpha^{\mathbf{f}},\varepsilon)}$ with initial condition $(q, \dot q) \in \mathcal{S}_{\mathbf{s}\to\mathbf{f}} \cap \mathbf{FZ}_{\alpha^{\mathbf{f}}}$, and $T_{\mathbf{f}}(q, \dot q)$ is the *time to impact function* [25] that determines the first time when the solution intersects the guard:

$$T_{\mathbf{f}}(q, \dot q) = \min\{t \in \mathbb{R}_{\geq 0} : \varphi_t^{\mathbf{f}}(q, \dot q) \in \mathcal{S}_{\mathbf{f}\to\mathbf{s}}\}. \quad (23)$$

Naturally, the problem stated as in (21), specifically due to the constraints (PHZD), is not in a form numerically solvable. Therefore, the objective of this section is to reframe this optimization problem in a way that is, at least, numerically solvable while provably resulting in robotic running.

Stance to Flight Constraints. In order to reframe (PHZD) in a way that can be numerically approached, we use the full hybrid zero dynamics surface to construct a point $(q, \dot q) \in \mathbf{FZ}_{\alpha^{\mathbf{s}}} \cap \mathcal{S}_{\mathbf{s}\to\mathbf{f}}$ that will be used as the initial condition in (22). To produce this point, we begin by assuming that the height of the foot is equal to some additional parameter α_{nsf} (which is allowed to be optimized). Therefore, we expand our set of parameters by defining $\beta_{\mathbf{f}} := (\alpha_{\mathbf{f}}, \alpha_{nsf})$. Using these parameters, a point $(\vartheta(\beta_{\mathbf{f}}), \dot\vartheta(\beta_{\mathbf{f}}))$ dependent on these parameters can be obtained by solving the equations:

$$\vartheta(\beta_{\mathbf{f}}) := \theta \quad \text{s.t} \quad \begin{bmatrix} y_2^{\mathbf{f}}(\theta) \\ h_{ns}(\theta) - \alpha_{nsf} \end{bmatrix} = \begin{bmatrix} \mathbf{0}_{3\times 1} \\ 0 \end{bmatrix},$$

$$\dot\vartheta(\beta_{\mathbf{f}}) = \begin{bmatrix} d\delta p_{\mathrm{hip}}(\vartheta(\beta_{\mathbf{f}})) \\ dy_2^{\mathbf{f}}(\vartheta(\beta_{\mathbf{f}})) \end{bmatrix}^{-1} \begin{bmatrix} v_{\mathrm{hip}} \\ \mathbf{0}_{3\times 1} \end{bmatrix}, \quad (24)$$

With this point in hand, we begin to construct the constraints by noting that at the moment $(\vartheta(\beta_{\mathbf{f}}), \dot\vartheta(\beta_{\mathbf{f}})) \in \mathcal{S}_{\mathbf{s}\to\mathbf{f}}$, it should follow:

$$\lambda(\vartheta(\beta_{\mathbf{f}}), \dot\vartheta(\beta_{\mathbf{f}})) = 0 \quad \text{(C1)}$$

which simply means that the Lagrangian Multiplier is crossing zero when the stance foot leaves the ground. Moreover, because of that $\Delta_{\mathbf{s}\to\mathbf{f}} = I$ and (C1) implies that $\tau_{\mathbf{f}}(\vartheta(\beta_{\mathbf{f}})) = 0$, the continuous constraints of the stance to flight transition can be stated as:

$$y_2^d(\tau_{\mathbf{s}}(\vartheta(\beta_{\mathbf{f}})), \alpha_{\mathbf{s}}) = y_2^d(0, \alpha_{\mathbf{f}}), \quad \text{(C2)}$$

$$dy_2^{\mathbf{s}}(\vartheta(\beta_{\mathbf{f}}))\dot\vartheta(\beta_{\mathbf{f}}) = dy_2^{\mathbf{f}}(\vartheta(\beta_{\mathbf{f}}))\dot\vartheta(\beta_{\mathbf{f}}), \quad \text{(C3)}$$

which allows us to conclude:

Lemma 1: For $\alpha_{\mathbf{s}}$ and $\beta_{\mathbf{f}}$ such that (C1)-(C3) are satisfied, it follows that $(\vartheta(\beta_{\mathbf{f}}), \dot\vartheta(\beta_{\mathbf{f}})) \in \mathbf{FZ}_{\alpha^{\mathbf{s}}} \cap \mathcal{S}_{\mathbf{s}\to\mathbf{f}}$ and $(\vartheta(\beta_{\mathbf{f}}), \dot\vartheta(\beta_{\mathbf{f}})) \in \mathbf{PZ}_{\alpha^{\mathbf{f}}}$

Flight to Stance Constraints. From Lemma 1, we know that $(\vartheta(\beta_{\mathbf{f}}), \dot\vartheta(\beta_{\mathbf{f}})) \in \mathbf{FZ}_{\alpha^{\mathbf{s}}} \cap \mathcal{S}_{\mathbf{s}\to\mathbf{f}}$ and so this point corresponds to the final point in the stance phase. Since $\Delta_{\mathbf{s}\to\mathbf{f}} = I$, it follows that this will be the initial condidtition to the flight phase. Again, using $\varphi^{\mathbf{f}}$ to denote the solution to the vector field $f_{\mathbf{f}}^{(\alpha^{\mathbf{f}},\varepsilon)}$, we define the following point:

$$(\varphi(\beta_{\mathbf{f}}), \dot\varphi(\beta_{\mathbf{f}})) = \varphi^{\mathbf{f}}_{T_{\mathbf{f}}(\vartheta(\beta_{\mathbf{f}}),\dot\vartheta(\beta_{\mathbf{f}}))}(\vartheta(\beta_{\mathbf{f}}), \dot\vartheta(\beta_{\mathbf{f}})) \quad (25)$$

with $T_{\mathbf{f}}$ in (23). Therefore, clearly $(\varphi(\beta_{\mathbf{f}}), \dot\varphi(\beta_{\mathbf{f}})) \in \mathcal{S}_{\mathbf{f}\to\mathbf{s}}$ and, in fact, by the invariance of $\mathbf{PZ}_{\alpha^{\mathbf{f}}}$ for the continuous dynamics $(\varphi(\beta_{\mathbf{f}}), \dot\varphi(\beta_{\mathbf{f}})) \in \mathbf{PZ}_{\alpha^{\mathbf{f}}} \cap \mathcal{S}_{\mathbf{f}\to\mathbf{s}}$ (from Lemma 1). The goal is to give constraints that ensure that, post-impact, $(\varphi(\beta_{\mathbf{f}}), \dot\varphi(\beta_{\mathbf{f}})) \in \mathbf{PZ}_{\alpha^{\mathbf{s}}}$, which are clearly implied as:

$$y_2^{\mathbf{s}}(\Delta_q\varphi(\beta_{\mathbf{f}})) = \mathbf{0} \quad \text{(C4)}$$

$$dy_2^{\mathbf{s}}(\Delta_q\varphi(\beta_{\mathbf{f}}))\Delta_{\dot q}\dot\varphi(\beta_{\mathbf{f}}) = \mathbf{0} \quad \text{(C5)}$$

$$dh_{ns}(\varphi(\beta_{\mathbf{f}}))\dot\varphi(\beta_{\mathbf{f}}) < 0 \quad \text{(C6)}$$

where (C6) implies the impact is "transverse" to the guard.

Main Result. We now have the necessary framework in which to introduce the *human-inspired optimization problem for running*:

$$\beta^* = \underset{\beta \in \mathbb{R}^{32}}{\operatorname{argmin}} \ \operatorname{Cost}_{\mathrm{HD}}(\beta) \tag{HIO}$$

$$\text{s.t} \quad (C1) - (C6). \tag{C}$$

where $\beta = (v_{\mathrm{hip}}, \alpha_{\mathbf{s}}, \beta_{\mathbf{f}})$, i.e., β consists of the parameters α and the parameter α_{nsf}; thus, any function of α can be viewed as a function of β in the obvious manner.

The goal is to show that if the constraints (C) are satisfied then it implies stable robotic running. Before proving this, some terminology is needed. For a point $(q, \dot{q}) \in \mathcal{S}_{\mathbf{s} \to \mathbf{f}}$, we can define the Poincaré map $P : \mathcal{S}_{\mathbf{s} \to \mathbf{f}} \to \mathcal{S}_{\mathbf{s} \to \mathbf{f}}$ which is a partial function:

$$P(q, \dot{q}) = \varphi^{\mathbf{s}}_{T_{\mathbf{s}}(\Delta_{\mathbf{s} \to \mathbf{s}}(q, \dot{q}))}(\Delta_{\mathbf{s} \to \mathbf{s}}(q, \dot{q})) \tag{26}$$

with $\Delta_{\mathbf{s} \to \mathbf{s}}$ as in (22), $\varphi^{\mathbf{s}}$ the flow of $f_{\mathbf{s}}^{(\alpha^{\mathbf{s}}, \varepsilon)}$ and $T_{\mathbf{s}}$ the time-to-impact function for the stance domain defined analogously to $T_{\mathbf{f}}$ as in (23). A running gait corresponds to a fixed point of P, i.e., $(q^*, \dot{q}^*) \in \mathcal{S}_{\mathbf{s} \to \mathbf{f}}$ such that $(q^*, \dot{q}^*) = P(q^*, \dot{q}^*)$ which implies that the hybrid system $\mathcal{H}_{(\beta, \varepsilon)}$ has a periodic orbit. A running gait is exponentially stable if P is exponentially stable as a discrete-time dynamical system, which in turn implies that the corresponding periodic orbit is exponentially stable [25]. With this notation in hand, we can state the main result of this paper which is a straight forward combination of Lemma 1, Theorem 1 in [4] and Theorem 2 in [3].

Theorem 1: *Let β^* be parameters solving* (HIO)*, then if* (C) *is satisfied, it implies partial hybrid zero dynamics* (PHZD). *Moreover, if $\tau_{\mathbf{s}}(\varphi(\beta_{\mathbf{f}}^*)) > 0$ then there exists a constant $\bar{\varepsilon} > 0$ such that for all $\varepsilon > \bar{\varepsilon}$, the hybrid system $\mathcal{H}_{(\beta, \varepsilon)}$ has an exponentially stable periodic orbit. Morover, the fixed point of this orbit, $(q_{\varepsilon}^*, \dot{q}_{\varepsilon}^*)$, is dependent on ε and satisfies the property that:*

$$\lim_{\varepsilon \to \infty}(q_{\varepsilon}^*, \dot{q}_{\varepsilon}^*) = (\vartheta(\beta_{\mathbf{f}}^*), \dot{\vartheta}(\beta_{\mathbf{f}}^*))$$

VI. SIMULATION RESULTS AND CONCLUSION

A simulation of the running with the control parameters obtained from the optimization problem (HIO) was performed. The actual outputs vs desired outputs over four steps are plotted in Fig. 7(b), from which we can see that outputs

(a) Hip Position   (b) Hip Angle

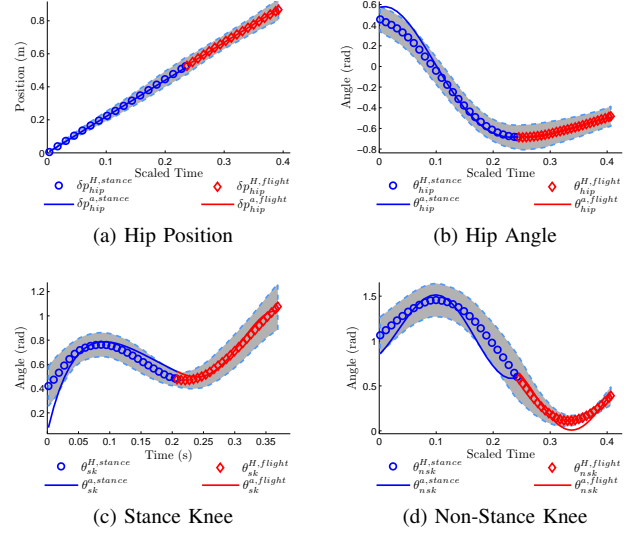(c) Stance Knee   (d) Non-Stance Knee

Fig. 6: Optimized canonical human functions (solid) and the corresponding mean human data of running (dashed).

of the robot agree with the desired outputs (for all but the velocity of the hip) implying that the relative degree 2 outputs are invariant through impact, i.e., we have achieved partial hybrid zero dynamics.

To quantify how "human-like" the running is, we also plot the actual outputs (with 42% flight phase duration) vs. the human experimental running data (with 37% flight phase duration), which can be seen in Fig. 6. Note that, the trajectories that fall into the one standard deviation boundary of mean human data (the region shown in the figure), are considered to be qualitative human-like . Also, the high correlations for each outputs along with the cost can be referred in Table. II. The running gaits of both phases achieved in simulation can be seen in Fig. 7(c), 7(d) and the video of the simulation results can be seen [2]. Readers may observe that the foot clearance of the flight phase is not very high. Comparing with mean human data, we found out that the foot clearance for mean human data is also quite low (most probably due to the constrained environment in which the running was performed). The swing foot height at the beginning of stance phase is $0.039m$ for the robot compared to $0.0415m$ for human; and the swing foot at the beginning of flight phase is $0.113m$ compared to human's $0.0985m$.
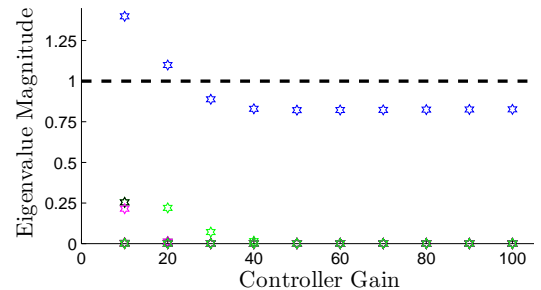
TABLE II: Optimized parameter values with human functions for mean data

		$y_1^a = v_{hip}t$,	$y_2^a = y_H(t)$ given in (1)					
		v_{hip}	α_1	α_2	α_3	α_4	α_5	Corr	Cost
Mean	δp_{hip}^{stance}	2.1998	*	*	*	*	*	0.9999	*
*	δp_{hip}^{flight}	2.1998	*	*	*	*	*	0.9999	*
*	θ_{hip}^{stance}	*	4.952	0.941	14.06	0.475	-0.370	0.9987	*
*	θ_{hip}^{flight}	*	13.04	-0.322	2.175	-2.828	-0.339	0.9960	*
*	θ_{sk}^{stance}	*	11.66	-0.159	3.153	6.561	0.196	0.8491	*
*	θ_{sk}^{flight}	*	-6.647	-0.119	24.98	-0.069	0.660	0.9911	*
*	θ_{nsk}^{stance}	*	-1.319	-0.241	23.55	0.284	1.089	0.9630	*
*	θ_{nsk}^{flight}	*	0.855	0.301	25.46	-0.242	0.364	0.9910	3.02

Fig. 8: Eigenvalues with controller gain $\varepsilon \in [10, 100]$

(a) Periodic Orbit (b) Actual vs. Desired Outputs (c) Gait Tiles for stance phase (d) Gait Tiles for flight phase
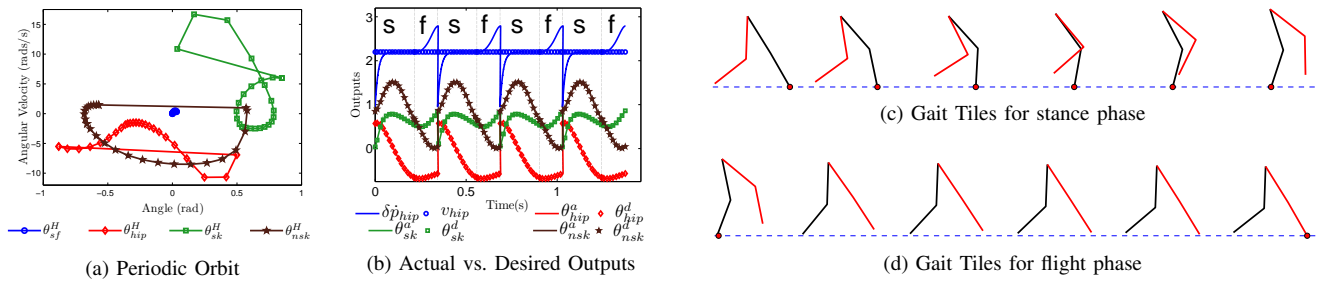
Fig. 7: Simulation Results, including: (a) the periodic orbit corresponding to the running gait, (b) the actual vs. desired outputs over 4 steps (with the stance and flight phase indicated) and (c),(d) gait tiles for the stance and flight phase.

Therefore, since we are seeking human-like running, we argue that the low foot clearance is a direct result of the human data from which the robotic running was derived.

From the discussion above, we can conclude that the optimized running gait achieves "human-like" running. The phase portraits are shown in Fig. 7(a) indicating that we do achieve a periodic orbit as Theorem 1 predicts. This theorem also predicts that this periodic orbit is stable for sufficiently large ε. In order to verify the stability of the running orbit, we construct numerical approximations of the Poincaré map (26) and check the eigenvalues. Fig. 8 shows how the poincare eigenvalues evolve with controller gain ε. With controller gain $\varepsilon = 30$, all eigenvalues have magnitude smaller than 1 with the maximum magnitude of 0.836 and we therefore numerically establish the stability of the running gait.

Conclusion. This paper studied bipedal robotic running in the context of human inspired control, providing yet another motion primitive [20] that can be described through this framework (adding to the existing collection consisting of walking on flat ground, up and down slopes and up and down stairs). Analysis of the experimental data shows that human running data, which consists of two phases, can also be represented by the response of a linear spring-mass-damper system, i.e., by the canonical locomotion function. We construct a novel optimization problem with constraints that ensure partial hybrid zero dynamics constraints for multiple domains. We establish that by solving this optimization problem, the end result is control parameters, i.e., parameters of the canonical locomotion functions, that provably result in stable robotic running. These formal results are verified through simulation. Future work will be devoted to realizing the results of this work on a physical robot.

REFERENCES

[1] Honda asimo running. http://youtu.be/FAcgSi6pzv4.
[2] Simulations of running. http://youtu.be/3X3wGOSLywg.
[3] A. Ames, E. Cousineau, and M. Powell. Dynamically stable bipedal robotic walking with nao via human-inspired hybrid zero dynamics. *In Hybrid Systems: Computation and Control*, 2012.
[4] A. D. Ames. *First Steps Toward Automatically Generating Bipedal Robotic Walking from Human Data*, volume 422 of *LNICS*. Springer.
[5] A. D. Ames, R. Vasudevan, and R. Bajcsy. Human-data based cost of bipedal robotic walking. *IEEE: HSCC*, 2011.
[6] G. A. Bekey. *Autonomous robots: from biological inspiration to implementation and control*. MIT Press, May 2005.
[7] R. Blickhan. The spring-mass model for running and hopping. *J. Biomechanics*, 22:1217–27.
[8] C. Chevallereau, E.R. Westervelt, and J.W. Grizzle. Asymptotically stable running for a five-link, four-actuator, planar bipedal robot. *International Journal of Robotics Research*, 24:431 – 464, 2005.
[9] H. Geyer, A. Seyfarth, and R. Blickhan. Compliant leg behaviour explains basic dynamics of walking and running. *Proceedings of the royal society*, 2006.
[10] P. Holmes, R.J. Full, D.E. Koditschek, and J. Guckenheimer. The dynamics of legged locomotion: Models, analyses, and challenges. *SIAM Review*, 2006.
[11] Y. Hürmüzlü and D. B. Marghitu. Rigid body collions of planar kinematic chains with multiple contact points. *Intl. J. of Robotics Research*, 13(1):82–92, February 1994.
[12] S. Jiang, S. Patrick, H. Zhao, and A.D. Ames. Outputs of human walking for bipedal robotic controller design. *American Control Conference*, 2012.
[13] S. Kamran and A. M. Dollar. On the mechanics of the knee during the stance phase of the gait. *Knee The*, pages 934–940, 2011.
[14] D. Koepl and J.W. Hurst. Force control for planar spring-mass running. *IEEE IROS*, September 2011.
[15] S. Koushil, P. Hae-Won, and W. G. Jessy. Design and experimental implementation of a compliant hybrid zero dynamics controller with active force control for running on mabel. *ICRA*, 2012.
[16] T. Luksch, K. Berns, K. Mombaur, and G. Schultz. Using optimization techniques for the design. pages 1–12, 2007.
[17] T. McGeer. Passive bipedal running. *Biological Sciences*, 240:107–134, 1990.
[18] R. M. Murray, Z. Li, and S. S. Sastry. *A Mathematical Introduction to Robotic Manipulation*. CRC Press, Boca Raton, March 1994.
[19] R.R. Playter and M.H. Raibert. Control of a biped somersault in 3d. *Theory Machines Mechanisms*, page 669C674, 1992.
[20] M. Powell, H. Zhao, and A. Ames. Motion primitives for human-inspired bipedal robotic locomotion : Walking and stair climbing. *IEEE:ICRA*, 2012.
[21] M.H. Raibert. *Legged Robot that Balance*. MIT Presss, 1986.
[22] J. Rose and J. G. Gamble. *Human Walking*. Lippincott Williams & Wilkins, Philadelphia, December 2005.
[23] S. S. Sastry. *Nonlinear Systems: Analysis, Stability and Control*. Springer, New York, June 1999.
[24] R. W. Sinnet and A. D. Ames. 2D bipedal walking with knees and feet: A hybrid control approach. In *IEEE: CDC*, pages 3200–3207, Shanghai, December 2009.
[25] E. R. Westervelt, J. W. Grizzle, C. Chevallereau, J. H. Choi, and B. Morris. *Feedback Control of Dynamic Bipedal Robot Locomotion*. CRC Press, Boca Raton, June 2007.
[26] E. R. Westervelt, J. W. Grizzle, and D. E. Koditschek. Hybrid zero dynamics of planar biped walkers. *IEEE TAC*, 48:42–56, 2003.
[27] S. N. Yadukumar, M. Pasupuleti, and A. D. Ames. From formal methods to algorithmic implementation of human inspired control on bipedal robots. *In the Tenth International WAFR*, 2012.
[28] F. Yasutaka. Trajectory generation of biped running robot with minimum energy consumption. *IEEE ICRA*, 2004.